Nanoscale

Accepted Manuscript

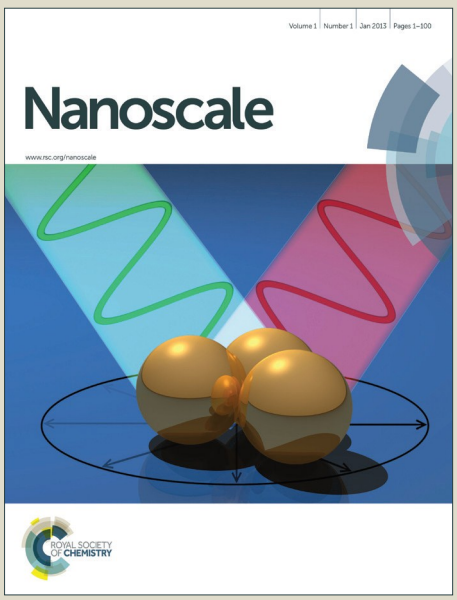

This is an *Accepted Manuscript*, which has been through the Royal Society of Chemistry peer review process and has been accepted for publication.

Accepted Manuscripts are published online shortly after acceptance, before technical editing, formatting and proof reading. Using this free service, authors can make their results available to the community, in citable form, before we publish the edited article. We will replace this *Accepted Manuscript* with the edited and formatted *Advance Article* as soon as it is available.

You can find more information about *Accepted Manuscripts* in the Information for Authors.

Please note that technical editing may introduce minor changes to the text and/or graphics, which may alter content. The journal's standard Terms & Conditions and the Ethical guidelines still apply. In no event shall the Royal Society of Chemistry be held responsible for any errors or omissions in this *Accepted Manuscript* or any consequences arising from the use of any information it contains.

ROYAL SOCIETY OF CHEMISTRY

www.rsc.org/nanoscale

Please do not adjust margins

Nanoscale

Communication

Nanoscale Mapping of Excitonic Processes in Single-layer MoS_2 using Tip-enhanced Photoluminescence Microscopy

Weitao Su[a, c], Naresh Kumar[b], Sandro Mignuzzi[b], Jason Crain[b,d], Debdulal Roy[b, †]

yReceived 00th January 20xx,
Accepted 00th January 20xx

DOI: 10.1039/x0xx00000x

www.rsc.org/

In two-dimensional semiconductors, photoluminescence originating from recombination processes involving neutral electron-hole pairs (excitons) and charged complexes (trions) is strongly affected by the localized charge transfer due to inhomogeneous interaction with the local environment and surface defects. Herein, we demonstrate the first nanoscale mapping of excitons and trions in single-layer MoS_2 using the full spectral information obtained via tip-enhanced photoluminescence (TEPL) microscopy along with tip-enhanced Raman spectroscopy (TERS) imaging of a 2D flake. Finally, we show mapping of PL quenching centre in single-layer MoS_2 with an unprecedented spatial resolution of 20 nm. In addition, our research shows that unlike in aperture-scanning near field microscopy, preferential exciton emission mapping at the nanoscale using TEPL and Raman mapping using TERS can be obtained simultaneously using this method that can be used to correlate structure and excitonic properties.

Single-layer molybdenum disulphide (MoS_2)[1], a member of two-dimensional (2D) dichalcogenides($MoSe_2$[2, 3], WS_2[4], GaTe[5], GaSe[6], etc.) with a hexagonal-layered lattice bonded by weak Van der Waals forces, has stimulated an enormous interest for applications in 2D optoelectronics(such as photodetectors[7, 8], solar cells[1] and light-emitting devices[1], etc.) because of the novel combination of electronic and optical properties. Unlike graphene which is a zero band-gap material with conical conduction and valence bands (Dirac cones) merging at the *K* point[9], the band structure of MoS_2 changes from indirect band in the bulk (band gap, $E_g \approx 1.2$ eV)[10] to a direct band ($E_g \approx 1.8$ eV)[11] in single-layer structure , which gives rise to a strong photoluminescence (PL) in single-layer MoS_2 through excitonic processes[12]. This PL emission consists of B-exciton band at 620 nm (2 eV) and A-exciton band at 670 nm (1.85 eV) which can be further assigned into neutral exciton ($A^0 \approx 1.88$ eV) and trion ($A^- \approx 1.84$ eV) sub-bands[11, 13]. The PL process in single-layer MoS_2 has been found to be strongly affected by the local environment such as substrate and capping layers[14-16], adsorbed molecules[13, 17-19] and defects[20-22]. Typically, these factors are present non-uniformly inside and on the surface of single-layer MoS_2 resulting in an inhomogeneous charge transfer that may greatly influence the local population of neutral (exciton) and charged (trion) quasi-particles[13]. Direct mapping of such local changes in exciton and trion populations is pivotal in excitonic devices such as excitonic interconnects[23, 24]. However, conventional optical techniques fail to map the variation in these excitonic processes in single-layer MoS_2 at the nanoscale due to the diffraction limit. Therefore, novel methods are required to probe the distribution of neutral exciton and trions at room temperature with a nanoscale resolution for applications in excitonic[24] and valleytronic devices[25].

Recently, aperture-based scanning near-field optical microscopy (a-SNOM) has been used by Lee *et al.*[26] and Bao *et al.*[27] to characterize the defects and boundaries in single-layer MoS_2 grown by chemical vapour deposited (CVD) with up to 60 nm spatial resolution. However, because of the limited size of the aperture, spatial resolution of a-SNOM (50 – 100 nm)[28, 29] is much larger than the exciton diffusion length (≈ 24 nm)[27, 30] and therefore, is insufficient to accurately probe the effect of structural defects and adsorbates on local excitonic processes on single-layer MoS_2 surface. On the other hand, tip-enhanced PL (TEPL) microscopy has been shown to be a powerful technique for nanoscale PL mapping in quantum dots[31] and organic molecules[32] with a high spatial resolution of 10 nm. TEPL microscopy is in principle quite similar to tip-enhanced Raman spectroscopy (TERS)[33, 34], which has been used for the nanoscale imaging of graphene[35, 36], single-wall carbon nanotubes[37], catalysis[38], semiconductors[39], biology[40], single molecules[41] etc. In TEPL microscopy, a metallic or a metal-coated scanning probe microscopy (SPM) tip is placed inside a laser focus, which generates localised surface plasmons (LSP) at the tip-apex. When LSP wavelength becomes resonant with the wavelength of excitation laser, a huge enhancement of electromagnetic (EM) field occurs at the tip-apex, which enhances the PL and Raman from the region immediately below the tip-apex enabling mapping of PL and Raman variation with a nanoscale resolution. To the best of our knowledge, the potential of TEPL microscopy to map the excitonic processes in 2D dichalcogenides like MoS_2, WS_2 etc., has not been reported yet. Herein, we report the first TEPL and TERS mapping of MoS_2 with nanoscale spatial resolution. We used an Ag-coated atomic force microscopy (AFM) tip and 532 nm excitation laser to map the excitons and trions in single-layer MoS_2 with a nanoscale

[a] *Institute of Materials Physics, Hangzhou Dianzi University, 310018, Hangzhou, China*
[b] *National Physical Laboratory, Hampton Road, Teddington, Middlesex, TW11 0LW, UK*
[c] *Key Laboratory of RF Circuits and Systems (Hangzhou Dianzi University), Ministry of Education of China.*
[d] *School of Physics and Astronomy, University of Edinburgh, James Clerk Maxwell Building, Peter Guthrie Tait Road, Edinburgh, EH9 3FD, UK*
*These authors contributed equally to this work
† Corresponding author: debdulal.roy@npl.co.uk
Electronic Supplementary Information (ESI) available: [details of any supplementary information available should be included here]. See DOI: 10.1039/x0xx00000x

Nanoscale Accepted Manuscript

resolution. Finally, we demonstrate mapping of PL quenching centre in single-layer MoS_2 with 20 nm spatial resolution using a TEPL set- up.

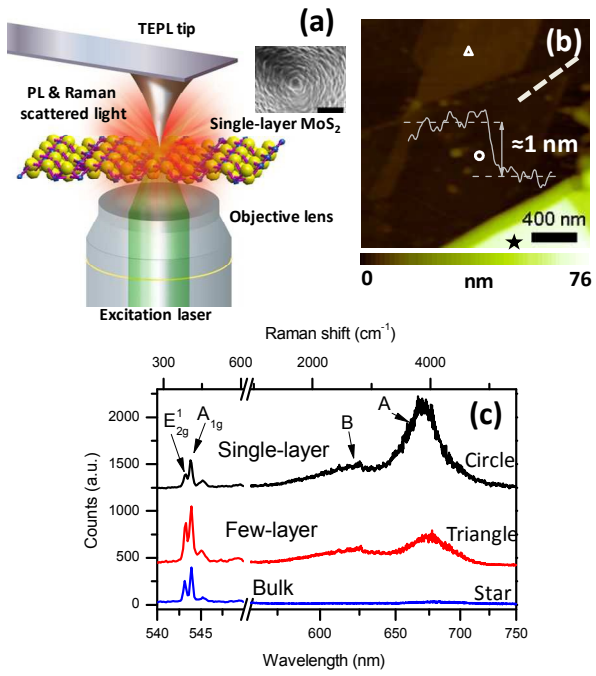

Figure 1 (a) Schematic diagram of the TEPL measurement set-up. SEM image of the Ag-coated AFM tip used in this work is shown in the inset. Scale bar = 200 nm. (b) AFM topography image of single-layer, few-layer and bulk MoS_2 flakes on a glass substrate. (c) Far-field Raman and PL spectra of the single-layer, few-layer and bulk-layer MoS_2 from the positions marked as circle, triangle and star in (b), respectively. Integration time:120 s.

In this work, all optical spectra measurements were acquired in transmission mode with a home-built set-up consisting of an inverted microscope (Nikon, Japan) fitted with an AFM (AIST-NT, The Netherlands) on top and a Raman spectrometer (HORIBA Scientific, UK) with an EMCCD camera (Andor, Ireland) at the side port. A schematic diagram of the measurement set-up is shown in Figure 1a. A radially polarised 532 nm laser was focused onto the sample using a 100× oil immersion objective lens (1.49 NA).Commonly used Scotch-tape method was used to prepare single-layer MoS_2 samples on glass coverslips (Thickness ≈ 0.17 mm)[12]. A laser power of 100 µW at the objective and an integration time of 0.5 s were used to collect the optical spectra in near-field (with the tip in contact with the sample) and far-field (the tip retracted from the sample) maps. Near-field PL and Raman mapping were carried out in contact-mode AFM using an Ag-coated tip, and the corresponding topography was measured in tapping-mode AFM. Ag-coated tips were prepared by coating thermally oxidized (300 nm SiO_2) silicon AFM cantilevers (MikroMasch, Estonia) with 100 nm Ag films by thermal evaporation in a vacuum chamber at a pressure of 10^{-6} mbar. Scanning electron microscopy (SEM) image of the Ag-coated AFM tip used in this work is shown in the inset of Figure 1a. Au-coated Si AFM tips were purchased commercially (Nanoworld, Switzerland).

AFM topography image of an area containing single-layer, few-layer, and bulk MoS_2 flakes is shown in Figure 1b. A cross-section profile along the dashed line in Figure 1b indicates that the height of the single-layer flake is ~ 1 nm, which is in good agreement with the values reported previously[16]. Figure 1c shows the far-field Raman and PL spectra measured from the positions marked on single-layer, few-layer and bulk MoS_2 in Figure 1b. Raman bands of in-plane E^1_{2g} and out-of plane A_{1g} vibration modes[42, 43] are observed at ~385 cm^{-1} and ~405 cm^{-1} in all optical spectra. However, A-exciton PL band at 670 nm (1.85 eV) and B-exciton PL band at 615 nm (2.02 eV) are observed in the spectra from the single-layer and few-layer MoS_2 flakes only. The PL intensity of few-layer MoS_2 decreases enormously from single-layer, while disappearing completely in bulk MoS_2 because of band structure transition from direct to indirect, which raises the intraband relaxation rate leading to a sharp drop of the quantum yield and PL intensity[44].

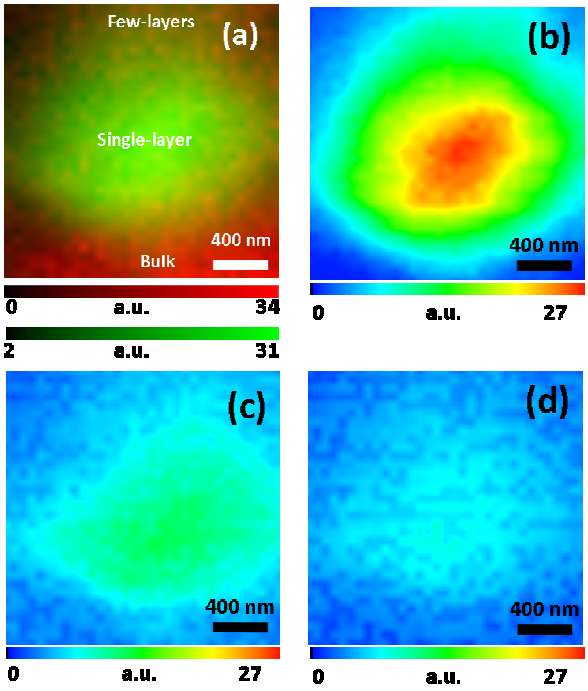

Figure 2 (a) Overlay image of far-field maps made using the intensity of A_{1g} Raman band (red) and A-exciton band (green) of 2 µm × 2 µm sample area shown in Figure 1b with 32 × 32 pixels. Deconvoluted far-field PL maps made using the intensity of (b) A^0 exciton, (c) A^- exciton (trion) and (d) B-exciton bands. Integration time: 0.5 s.

An overlay image of the far-field Raman and PL maps made using the intensity of A_{1g} Raman (red) and A-exciton PL bands (green), respectively of the MoS_2 sample in Figure 1b is shown in Figure 2a. In this overlay image, high green intensity areas represent the location of single-layer MoS_2, whereas high red intensity areas represent the location of bulk or few-layer MoS_2. Comparing Figure 2a to Figure 1b, it can be seen that single-layer can only be coarsely located by the brightest green intensity due to diffraction-limited spatial resolution. Moreover, no PL-related fine structure can be seen in single-layer MoS_2. As mentioned previously, PL in single-layer MoS_2 can be deconvoluted into A^0 exciton (660 nm), A^- exciton (trion) (673 nm) and B-exciton (615 nm) bands by fitting with three Gaussian peaks. These deconvoluted PL maps are shown in Figures 2c-2d, respectively. It can be seen that the PL intensity in single-layer MoS_2 is dominated by A^0 exciton. However, no variation at the

Nanoscale Accepted Manuscript

This journal is © The Royal Society of Chemistry 20xx

nanoscale in the intensity can be discerned in any of these exciton maps due to the diffraction-limited spatial resolution of confocal optical microscopy.

We first investigated the influence of Ag- and Au-coated tips on local excitonic processes and electron populations in single-layer MoS_2 (shown in Figure 3a and 3b, respectively). The optical spectra measured with an Ag-coated tip in contact (tip-in) and retracted (tip-out) from a single-layer MoS_2 flake are shown in Figure 3a. Two phenomena are observed in the near-field spectrum of Ag-coated tip: (1) The intensities of both Raman and PL A-exciton bands are enhanced. (2) The relative intensity of trions is enhanced in the A-exciton band as shown by the fitted spectra in Figure 3a. The first observation can be explained by the resonance of LSP energy of Ag-coated tips (≈ 2.4 eV)[45] with 532 nm excitation energy (2.3 eV) leading to a strong enhancement of EM field intensity at the tip-apex. This increase in the intensity of EM field at tip-apex causes a strong enhancement of both Raman and PL band intensities. Raman signal is enhanced by the fourth power of EM field intensity beneath the tip apex, while PL is affected by EM intensity, metal induced alteration of decay rate, quenching and doping[46]. The enhancement factors of A_{1g} Raman and A-exciton PL band are calculated to be 622 and 448 (See Supplementary Information section S1 for detail). The second observation can be explained by considering the work function of Ag (4.3 eV) [47] and single-layer MoS_2 (4.7 eV) [47], which is schematically shown in Figure 3c. Since the work function of Ag is lower than MoS_2, electrons flow from Ag to MoS_2 causing n-type doping, which is known to decrease the relative intensity of A^0 exciton[48] .

In contrast to Ag-coated tip, a very different impact on the excitonic processes is observed in the presence of an Au-coated tip on single-layer MoS_2. Figure 3b shows the tip-in and tip-out spectra in the presence and absence of an Au-coated tip on a different single-layer MoS_2 flake. Once again, two phenomena are observed in the tip-in spectrum: (1) Intensity of only the A-exciton band is enhanced, whereas the intensity of Raman remains unchanged. (2) The relative intensity of A^0 excitons in the A-exciton band is increased. The absence of enhancement of Raman bands also indicates there is no EM enhancement since the LSP energy of Au-coated tips (1.9 ev)[49] is not on resonance with 532 nm excitation energy (2.3 eV). This also indicates that the increase in the intensity of PL cannot arise from EM enhancement, but from charge transferring effect. As shown by the schematic diagram of the work functions of Au and single-layer MoS_2 in Figure 3c, the work function of MoS_2 (4.7 eV) is less than Au (5.1 eV)[50], which makes the electrons move from single-layer MoS_2 to Au-coated tip causing p-doping. This p-doping from the Au tip enhances the exciton-PL intensity only, while the trion-PL remains unchanged (observation 2) . Therefore, enhancement of the A^0-exciton PL occurs due to the *p*-doping by the Au-tip[16, 17]. Furthermore, in order to measure the effect of the metallic tips on local electron population we formulated the exciton generation, recombination, transformation from an exciton to a trion and subsequently its relaxation (see Supplementary Information section S2 for details). Using the PL-trion intensity fraction, previously reported for different degrees of electron doping[13], we estimated the electron population corresponding to tip-out and tip-in measurements for Ag- and Au-coated tips as shown in Figure 3d. The changes in electron population due to doping by the metallic tips are calculated to be -58% and 952% for Au and Ag tips, respectively. These values are of the same order of magnitude as observed before[13], and are consistent with our understanding that charge transfer between the tips and single-layer MoS_2 leads to enhancement or suppression of the PL emissions of different quasiparticles (excitons and trions). Attempt was made to measure the shift of the A_{1g} Raman mode which is affected by doping[51]; however, due to limited spectral resolution of these measurements a small degree of doping could not be detected from the peak shift.

Since Ag-coated tip showed a much stronger enhancement of Raman and PL signals in the near-field, we chose it for TEPL mapping of the single-layer MoS_2 flake in Figure 1b.

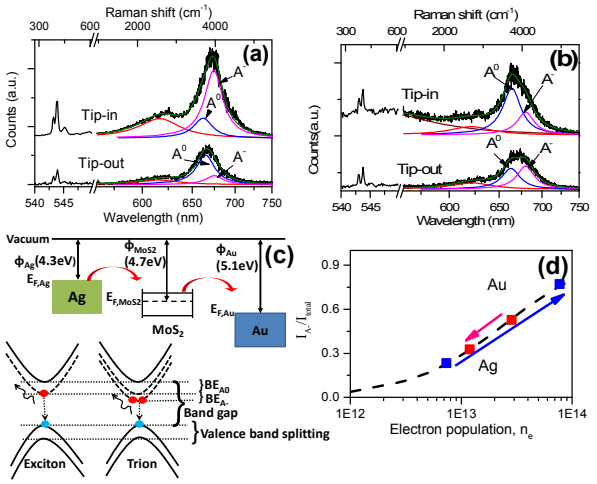

Figure 3 (a) Tip-in (near-field) and tip-out (far-field) spectra in the presence and absence of Ag-coated tip from single-layer MoS_2. The A^0, A^- and B-exciton PL intensity are fitted using the blue, pink and red curves, respectively. (b) Tip-in and tip-out spectra using Au-coated tip from single-layer MoS_2. The A^0, A^- and B-exciton PL intensity are fitted using the blue, pink and red curves, respectively (Please see Figure S1 of suppmentary information for the stacked PL curves, and Figure S2 of supplementary information for the emission band of Au-and Ag-coated tips). (c) Schematic diagram showing the work function of MoS_2, Ag and Au and depicting the charge transfer processes. (bottom) A schematic diagram of exciton- and trion-related radiative transition at the K-point in the Brillouin zone.BE_{A0} and BE_{A-} denote the excitonic binding energy of exciton and trion, respectively. (d) Electron population calculated from the relative intensities of trion-PL and A^0 exciton-PL using the formulation described in the Supplementary Information.

The TEPL maps are shown in Figure 4. Figure 4a shows an overlay image of the maps of A_{1g} Raman band intensity (red) and A-exciton PL band intensity (green) in the near-field of Ag-coated tip. It can be immediately seen that this near-field image is sharper than the confocal image in Figure 2a due the higher spatial resolution offered by TEPL. The few-layer and bulk layer, which have weaker PL signals, can be clearly identified by the brighter red in TERS A_{1g} map, while the single-layer, which has weaker Raman signal can be identified by brighter green in the PL map. The boundaries between different MoS_2 flakes can now be clearly distinguished and the shape and size of the triangular single-layer MoS_2 flake correlate perfectly with the AFM topography image in Figure 1b where the single layer MoS_2 flake can be hardly distinguished from the glass background due to < 1 nm height. The near-field intensity maps of A^0-exciton, A^--exciton (trion) and B-exciton bands are shown in Figures 4b–4d, respectively. It can be seen that as compared to the far-field deconvoluted PL maps in Figures 2b – 2d, the trion and B-exciton PL intensity is enhanced, whereas the A^--exciton PL intensity is quenched in the near-field maps. Furthermore, PL intensity in the near-field is dominated by trion PL. As compared to the distribution of A^0-exciton PL (Figure 4b), trion (Figure 4c) and B-exciton PL

Nanoscale Accepted Manuscript

(Figure 4d) are distributed relatively more uniformly indicating a uniform EM enhancement throughout the single-layer MoS_2 flake in the near-field of Ag-coated tip. However, the upper-half of Figure 4b has a much stronger A^0-exciton intensity compared to the lower-half. This non-uniform distribution of A^0-exciton intensity could arise from the charge transfer from inhomogeneities such as structural defects in single-layer MoS_2, chemical doping by surface contamination or the glass substrate.

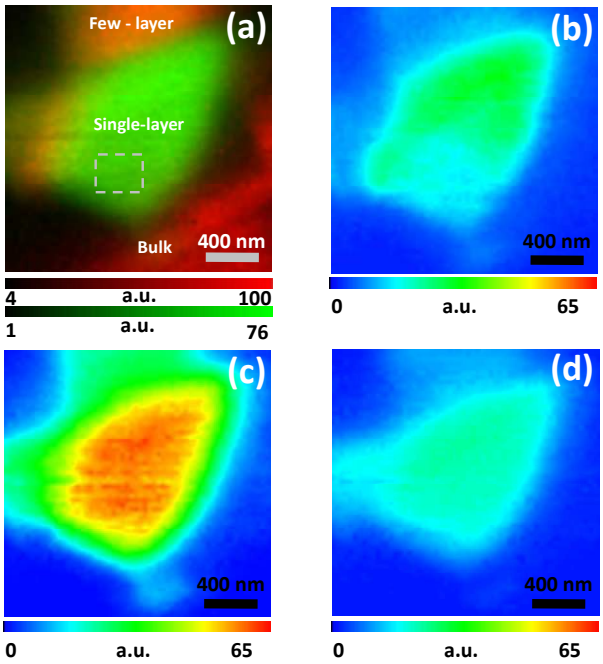

Figure 4 (a) Overlay image of TERS map obtained using the A_{1g} Raman band intensity (red) and TEPL map obtained using the A-exciton band intensity (green) from 2 µm × 2 µm single-layer MoS_2 area shown in Figure 1b with 60 × 60 pixels. (b) A^0 exciton PL map, (c) trion PL map and (d) B-exciton map deconvoluted from the PL spectra measured at each pixel in the near-field of the Ag-coated tip.

These nanoscale variations in the A^0 exciton maps can't be observed in the far-field image (Figure 2b). The nanoscale spatial resolution of TEPL imaging can only be accurately determined by zoomed-in map shown in the following part. In contrast to a-SNOM, the TEPL mapping allows full spectral information to be obtained at each pixel with a nanoscale spatial resolution, which can be carefully fitted to obtain information about the distribution of exciton and trion quasiparticles intensity in single-layer MoS_2.

A higher resolution TEPL map was acquired with pixel size of 10nm from a 250 nm × 200 nm area marked by dotted rectangle in Figure 4a(See part S5 for the comparison of average tip-in and tip-out spectra from this area). TEPL maps obtained using PL intensities of B-, A^0- and A^--excitons are shown in Figure 5(a), (b) and (c), respectively. In these maps, a low PL intensity region of size 90 nm × 40 nm can be identified in the single-layer. This low PL area is observed at the same position with nearly same shape, which indicates the PL intensities of all the three excitons are quenched by the same quenching centre. This quenching centre most probably arises from the structural defects, surface contamination or inhomogeneous charge transfer between single-layer MoS_2 and the glass substrate[48]. Spatial resolution of this map can be determined from the intensity profile across the quenching area in Figure 5c. As shown in Figure 5d, the spatial resolution of the TEPL map is determined from the width at half maximum of the slope to be 20 nm, which is 18 times better than the confocal spatial resolution of our microscope (370 nm) and 25 times smaller than the excitation wavelength (532 nm). Furthermore, the spatial resolution in this TEPL map is 5 times better than that of a-SNOM obtained by Lee et al [26] and 3 times better than that reported by Bao et al[27]. This indicates that PL

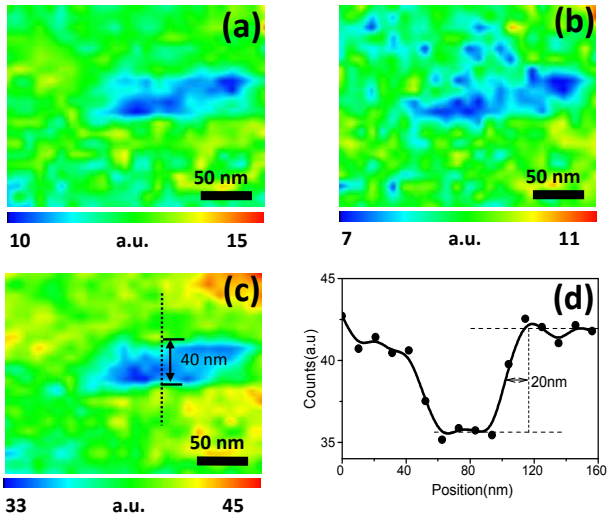

Figure 5 Zoomed-in TEPL maps of (a) B exciton,(b)A^0 exciton and (c)A^- exciton (25 x 20 pixels), showing a PL quenching centre on a single-layer MoS_2 flake from the acrea marked with dashed rectangle in Figure 4(a). (f) Calculation of spatial resolution of TEPL map from the intensity profile along the dashed line in (c).

mapping of growth-related defects, such as sulphur-deficient boundaries and edges in single layer MoS_2 with a much higher lateral resolution is possible using TEPL.

In conclusion, in this work we have carried out the first nanoscale TEPL and TERS mapping of MoS_2. We investigated the influence of Ag- and Au-coated AFM tips on local excitonic processes and electonic population in single-layer MoS_2 and found them to significantly affected by the work function of the metals. Using an Ag-coated tip we demonstrated TEPL mapping of A^0, A^- and B-excitons in a single-layer MoS_2 with a nanoscale resolution Nanoscale TERS mapping of MoS_2 were also obtained simultaneously with TEPL imaging . These nanoscale TEPL and TERS imaging cannot be achieved either by far-field optical techniques or a-SNOM. Finally, we showed mapping of PL variation inside a single-layer MoS_2 flake with an unprecendented 20 nm spatial resolution, which is 18 times better than the confocal optical resolution and 25 times smaller than the excitation wavelength used. These novel measurements demonstrate the potential of TEPL microscopy to characterize local excitonic processes in single-layer 2D semiconducting materials, which is expected to pave the way for development of nanoscale optoelectronic and excitonic devices.

Acknowledgements

WS acknowledges the financial support from Natural Sciences Foundation of China (Grant No: 61306115 and 61178039), China

Nanoscale Accepted Manuscript

This journal is © The Royal Society of Chemistry 20xx

Postdoctoral Science Foundation (Grant No. 2013M541807) and the international secondment scheme from NPL. NK acknowledges financial support from the IRD Graphene project of the National Measurement System of the UK Department of Business, Innovation and Skills. DR acknowledges financial support from the EMRP NEW02 project 'Metrology for Raman spectroscopy'. EMRP is jointly funded by the participating countries within EURAMET and the European Union.

Notes and references

1. O. Sanchez Lopez, E. A. Llado, V. Koman, A. F. Morral, A. Radenovic and K. Andras, *Acs Nano*, 2014, 8, 3042-3048.
2. Y. Gong, S. Lei, G. Ye, B. Li, Y. He, K. Keyshar, X. Zhang, Q. Wang, J. Lou, Z. Liu, R. Vajtai, W. Zhou and P. M. Ajayan, *Nano Letters*, 2015, 15, 6135-6141.
3. W. J. Zhao, Z. Ghorannevis, L. Q. Chu, M. L. Toh, C. Kloc, P. H. Tan and G. Eda, *Acs Nano*, 2013, 7, 791-797.
4. A. Molina-Sanchez and L. Wirtz, *Physical Review B*, 2011, 84.
5. X. Yuan, L. Tang, P. Wang, Z. Chen, Y. Zou, X. Su, C. Zhang, Y. Liu, W. Wang, C. Liu, F. Chen, J. Zou, P. Zhou, W. Hu and F. Xiu, *Nano Res.*, 2015, 8, 3332-3341.
6. X. Yuan, L. Tang, S. Liu, P. Wang, Z. Chen, C. Zhang, Y. Liu, W. Wang, Y. Zou, C. Liu, N. Guo, J. Zou, P. Zhou, W. Hu and F. Xiu, *Nano Letters*, 2015, 15, 3571-3577.
7. J. Miao, W. Hu, Y. Jing, W. Luo, L. Liao, A. Pan, S. Wu, J. Cheng, X. Chen and W. Lu, *Small*, 2015, 11, 2346-2346.
8. X. Wang, P. Wang, J. Wang, W. Hu, X. Zhou, N. Guo, H. Huang, S. Sun, H. Shen, T. Lin, M. Tang, L. Liao, A. Jiang, J. Sun, X. Meng, X. Chen, W. Lu and J. Chu, *Advanced Materials*, 2015, n/a-n/a.
9. K. S. Novoselov, A. K. Geim, S. V. Morozov, D. Jiang, Y. Zhang, S. V. Dubonos, I. V. Grigorieva and A. A. Firsov, *Science*, 2004, 306, 666-669.
10. K. K. Kam and B. A. Parkinson, *Journal of Physical Chemistry*, 1982, 86, 463-467.
11. K. F. Mak, C. Lee, J. Hone, J. Shan and T. F. Heinz, *Phys. Rev. Lett.*, 2010, 105, 136805.
12. A. Splendiani, L. Sun, Y. Zhang, T. Li, J. Kim, C. Y. Chim, G. Galli and F. Wang, *Nano Lett.*, 2010, 10, 1271-1275.
13. S. Mouri, Y. Miyauchi and K. Matsuda, *Nano Lett.*, 2013, 13, 5944-5948.
14. H. P. Komsa and A. V. Krasheninnikov, *Phys. Rev. B.*, 2012, 86, 6.
15. D. Sercombe, S. Schwarz, I. I. Tartakovskii, O. Kolosov, O. D. Pozo-Zamudio, F. Liu, B. J. Robinson, E. A. Chekhovich and A. I. Tartakovskii, *Sci. Rep.*, 2013, 3, 3489.
16. M. Buscema, G. A. Steele, H. S. J. van der Zant and A. Castellanos-Gomez, *Nano Res.*, 2014, 7, 561-571.
17. W. Su, H. Dou, D. Huo, N. Dai and L. Yang, *Chemical Physics Letters*, 2015, 635, 40-44.
18. W. Su, H. Dou, J. Li, D. Huo, N. Dai and L. Yang, *RSC Advances*, 2015, 5, 82924-82929.
19. W. Su, N. Kumar, N. Dai and D. Roy, *Nano Res.*, 2015, DOI 10.1007/s12274 - 015 - 0887 - 7, paper in publishing.
20. K. F. Mak, K. He, C. Lee, G. H. Lee, J. Hone, T. F. Heinz and J. Shan, *Nat. Mater.*, 2013, 12, 207-211.
21. J. S. Ross, S. F. Wu, H. Y. Yu, N. J. Ghimire, A. M. Jones, G. Aivazian, J. Q. Yan, D. G. Mandrus, D. Xiao, W. Yao and X. D. Xu, *Nat. Commun.*, 2013, 4, 6.
22. S. Tongay, J. Zhou, C. Ataca, J. Liu, J. S. Kang, T. S. Matthews, L. You, J. B. Li, J. C. Grossman and J. Q. Wu, *Nano Lett.*, 2013, 13, 2831-2836.
23. M. Baldo and V. Stojanovic, *Nat Photon*, 2009, 3, 558-560.
24. P. Andreakou, S. V. Poltavtsev, J. R. Leonard, E. V. Calman, M. Remeika, Y. Y. Kuznetsova, L. V. Butov, J. Wilkes, M. Hanson and A. C. Gossard, *Applied Physics Letters*, 2014, 104, 091101.
25. K. F. Mak, K. He, J. Shan and T. F. Heinz, *Nature Nanotechnology*, 2012, 7, 494-498.
26. Y. Lee, S. Park, H. Kim, G. H. Han, Y. H. Lee and J. Kim, *Nanoscale*, 2015, 7, 11909-11914.
27. W. Bao, N. J. Borys, C. Ko, J. Suh, W. Fan, A. Thron, Y. Zhang, A. Buyanin, J. Zhang, S. Cabrini, P. D. Ashby, A. Weber-Bargioni, S. Tongay, S. Aloni, D. F. Ogletree, J. Wu, M. B. Salmeron and P. J. Schuck, *Nat Commun*, 2015, 6, 7993.
28. B. Hecht, B. Sick, U. P. Wild, V. Deckert, R. Zenobi, O. J. F. Martin and D. W. Pohl, *The Journal of Chemical Physics*, 2000, 112, 7761-7774.
29. D. Roy, S. H. Leong and M. E. Welland, *Journal of the Korean Physical Society*, 2005, 47, S140-S146.
30. A. M. van der Zande, P. Y. Huang, D. A. Chenet, T. C. Berkelbach, Y. You, G.-H. Lee, T. F. Heinz, D. R. Reichman, D. A. Muller and J. C. Hone, *Nat Mater*, 2013, 12, 554-561.
31. H. Fu Min and D. Richards, *Journal of Optics A: Pure and Applied Optics*, 2006, 8, S234-238.
32. D. Zhang, U. Heinemeyer, C. Stanciu, M. Sackrow, K. Braun, L. E. Hennemann, X. Wang, R. Scholz, F. Schreiber and A. J. Meixner, *Physical Review Letters*, 2010, 104, 056601.
33. C. Blum, L. Opilik, J. M. Atkin, K. Braun, S. B. Kämmer, V. Kravtsov, N. Kumar, S. Lemeshko, J. F. Li and K. Luszcz, *Journal of Raman Spectroscopy*, 2014, 45, 22-31.
34. N. Kumar, S. Mignuzzi, W. Su and D. Roy, *EPJ Techniques and Instrumentation*, 2015, 2, 1-23.
35. W. Su and D. Roy, *J. Vac. Sci. Technol., B*, 2013, 31, 041808.
36. A. J. Pollard, N. Kumar, A. Rae, S. Mignuzzi, W. Su and D. Roy, *Journal of Materials NanoScience*, 2014, 1, 39-49.
37. Y. Okuno, Y. Saito, S. Kawata and P. Verma, *Phys. Rev. Lett.*, 2013, 111, 216101.
38. N. Kumar, B. Stephanidis, R. Zenobi, A. Wain and D. Roy, *Nanoscale*, 2015, 7, 7133-7137.
39. N. Lee, R. D. Hartschuh, D. Mehtani, A. Kisliuk, J. F. Maguire, M. Green, M. D. Foster and A. P. Sokolov, *J. Raman Spectrosc.*, 2007, 38, 789-796.
40. S. Najjar, D. Talaga, L. Schue, Y. Coffinier, S. Szunerits, R. Boukherroub, L. Servant, V. Rodriguez and S. Bonhommeau, *J. Phys. Chem. C*, 2014, 118, 1174-1181.
41. R. Zhang, Y. Zhang, Z. C. Dong, S. Jiang, C. Zhang, L. G. Chen, L. Zhang, Y. Liao, J. Aizpurua, Y. Luo, J. L. Yang and J. G. Hou, *Nature*, 2013, 498, 82-86.
42. C. Lee, H. Yan, L. E. Brus, T. F. Heinz, J. Hone and S. Ryu, *Acs Nano*, 2010, 4, 2695-2700.
43. A. Molina-Sanchez and L. Wirtz, *Phys. Rev. B.*, 2011, 84, 8.
44. A. Splendiani, L. Sun, Y. Zhang, T. Li, J. Kim, C.-Y. Chim, G. Galli and F. Wang, *Nano Letters*, 2010, 10, 1271-1275.
45. J. Stadler, T. Schmid and R. Zenobi, *Acs Nano*, 2011, 5, 8442-8448.
46. C. Gong, C. Huang, J. Miller, L. Cheng, Y. Hao, D. Cobden, J. Kim, R. S. Ruoff, R. M. Wallace, K. Cho, X. Xu and Y. J. Chabal, *ACS Nano*, 2013, 7, 11350-11357.
47. S. Mouri, Y. Miyauchi and K. Matsuda, *Nano Letters*, 2013, 13, 5944-5948.

Nanoscale Accepted Manuscript

48. M. Zhang, R. Wang, Z. Zhu, J. Wang and Q. Tian, *J. Opt.*, 2013, 15, 055006.
49. H. B. Michaelson, *J. Appl. Phys.*, 1977, 48, 4729-4733.
50. B. Chakraborty, A. Bera, D. V. S. Muthu, S. Bhowmick, U. V. Waghmare and A. K. Sood, *Physical Review B*, 2012, 85.
51. N. Kumar, A. Rae and D. Roy, *Appl. Phys. Lett.*, 2014, 104, 123106.
52. J. Siviniant, D. Scalbert, A. V. Kavokin, D. Coquillat and J. P. Lascaray, *Phys. Rev. B.*, 1999, 59, 1602-1604.
53. T. Cheiwchanchamnangij and W. R. L. Lambrecht, *Phys. Rev. B.*, 2012, 85.

Nanoscale Accepted Manuscript

This journal is © The Royal Society of Chemistry 20xx

Please do not adjust margins

Nanoscale Accepted Manuscript